

# Towards Online Observability-Aware Trajectory Optimization for Landmark-based Estimators

Kristoffer Frey<sup>1,2</sup>, Ted Steiner<sup>2</sup>, and Jonathan P. How<sup>1</sup>

<sup>1</sup> Massachusetts Institute of Technology, Cambridge MA 02139, USA,  
kfrey,jhow@mit.edu

<sup>2</sup> Charles Stark Draper Laboratory, Cambridge MA 02139, USA,  
tsteiner@draper.com

**Abstract.** As autonomous systems rely increasingly on onboard sensors for localization and perception, the parallel tasks of motion planning and uncertainty minimization become increasingly coupled. This coupling is well-captured by augmenting the planning objective with a posterior-covariance penalty – however, online optimization can be computationally intractable, particularly for observation models with latent environmental dependencies (e.g., unknown landmarks). This paper addresses a number of fundamental challenges in efficient minimization of the posterior covariance. First, we provide a measurement bundling approximation that enables high-rate sensors to be approximated with fewer, low-rate updates. This allows for landmark *marginalization* (crucial in the case of unknown landmarks), for which we provide a novel recipe for computing the gradients necessary for optimization. Finally, we identify a large class of measurement models for which the contributions from each landmark can be combined, so evaluation of the total information gained at each timestep can be carried out (nearly) independently of the number of landmarks. We evaluate our trajectory-generation framework for both a Dubin’s car and a quadrotor, demonstrating significant estimation improvement and moderate computation time.

**Keywords:** observability, belief-space planning, trajectory optimization

## 1 Introduction

In the last decade, significant progress has been made to enable basic autonomy for low-SWaP (Size, Weight, and Power) systems. Thanks to recent algorithmic advances, such systems can navigate purely from onboard sensors and avoid dependence on dedicated infrastructure such as GPS or motion-capture, allowing operation in a wider range of environments. However, commonly-used sensors such as IMUs, laser scanners, and cameras have nonlinear observation models and/or limited field-of-view (FoV), and thus the observability of the estimated state depends on the system trajectory. Furthermore, these sensors can have time-varying latent parameters (e.g., IMU biases, rigid-body calibrations) and environmental dependencies (e.g., the presence or absence of high-gradient corner features). Thus, even with a good initialization point and optimal estimation,

estimation performance may degrade to catastrophic levels if the chosen trajectory or environment does not provide sufficient information.

Conventional planning approaches [10] minimize energy or control effort along a trajectory, an objective that is often in tension with observability. While such approaches have shown some success in practice, estimation uncertainty can exceed safe thresholds without careful system calibration or if opportunistic landmarks do not exist at sufficient levels uniformly in the environment. However, maintaining calibrations for a fleet of vehicles can be onerous, and in many environments the distribution of landmarks is far from uniform. In these cases, designing trajectories that ensure good observability can produce significant localization improvement in general and may be the difference between mission success and failure.

A standard approach [2, 6, 15, 18, 19, 21] to this belief-space planning problem represents uncertainty as a Gaussian distribution about a nominal linear-time-varying (LTV) trajectory, providing a compact parametric representation of uncertainty. The corresponding covariance matrix is a *deterministic* function of the underlying trajectory, and does not depend on the random, and therefore unknown, realizations of future measurements. This crucial fact has enabled a number of approaches that minimize a time-varying Linear-Quadratic-Gaussian (LQG) cost, based on sampling [2, 15, 18], motion-primitives [4, 21], or continuous-optimization [6, 19]. However, sampling-based approaches are not well-suited for systems with more than a few degrees of freedom, and motion-primitive solutions do not address the fundamental issue of ensuring trajectories are well-observable in the first place. In the space of continuous trajectory generation, existing approaches have only been demonstrated with relatively simple sensor models [14, 16, 19] or scale poorly with large numbers of landmarks [6].

In order to avoid the computational complexity of explicit covariance minimization, heuristic approaches maximize an observability or (in the case of landmark-based systems) visibility metric. For example, [1, 3, 9] identify and enumerate non-observable trajectories to hand-design a discrete set of “well-observable” maneuvers for use in online planning. More recently, [13] leverages a reinforcement learning framework to select a sequence of primitive maneuvers in a manual calibration routine. From the side of continuous optimization, [8, 14] maximize observability metrics based on the Local Observability Gramian (LOG) in a continuous-optimization setting. For landmark-based systems with limited FoV (e.g., cameras), explicit visibility-based metrics have been used by [5] and [12] in real-time planning frameworks, with some success. However, heuristic methods ultimately fail to capture the full observability characteristics of the system, and therefore may select high-energy (expensive) trajectories with little corresponding estimation improvement [16].

A number of factors contribute to the computational complexity of exact posterior-covariance minimization. As the covariance must be propagated explicitly along the trajectory, the number of updates scales with the measurement rate, which can be undesirable for high-rate sensors such as cameras. Furthermore, landmark-based systems such as visual-SLAM can estimate tens or hun-

dreds of landmarks simultaneously. Besides having to compute the contribution from each of these landmarks (linear-complexity), exact representation of the joint belief state requires augmenting the covariance matrix for each landmark, an intractable quadratic growth in complexity.

### 1.1 Contributions

In this work, we address these challenges to enable efficient posterior-covariance minimization for a general class of landmark-based observation models.

- **Measurement bundling:** To avoid computing a full estimator update for every measurement timestep, in Section 3 we propose a bundling scheme that allows approximation of high-rate measurements with fewer, low-rate updates.
- **Handling unknown landmarks:** We avoid explicitly augmenting the covariance matrix (which would imply a quadratic complexity growth in the size of the map) by marginalizing out the landmark from each (bundled) measurement. As required for local optimization, we provide a convenient recipe for the gradient of the resulting information matrix  $\Lambda$  in Section 4.
- **Handling many landmarks:** In Section 6 we identify a broad class of observation models for which the contributions from multiple landmarks (accounting for field-of-view) can be compactly evaluated all together. This makes evaluation of a proposed trajectory largely invariant of the number of landmarks, facilitating efficient optimization even when reasoning against large clouds of landmarks. As compared to [22], which only applies to a particular observation and visibility model of *known* landmarks, our decomposition is much more general.

We numerically validate our measurement bundling approximation for both a Dubin’s car and quadrotor systems, demonstrating significant computational improvement with low approximation error. Our full trajectory generation pipeline is evaluated in a large number of random trials for both of these systems, demonstrating better estimation improvement than heuristic methods. Although our implementation is not yet fast enough for real-time operation, the improvements herein suggest that an online solution may be feasible in the near future.

## 2 Preliminaries

We assume the system state  $x$  lies on an  $n$ -dimensional manifold  $X$  with dynamics given by the stochastic ODE

$$\dot{x}(t) = f(x(t), u(t)) dt + G(x(t), u(t)) d\mathbf{w}(t) \in T_{x(t)}X, \quad (1)$$

where  $T_xX$  denotes the tangent space of  $X$  at the point  $x$ . The input  $u$  is confined to a set  $\mathcal{U}$ , and  $\mathbf{w}(\cdot)$  is a Brownian noise process with identity covariance. We assume measurements are acquired by a collection of sensors

$$dz_i = h(x; \ell_i) dt + d\boldsymbol{\nu}_i(t), \quad (2)$$

each corrupted by Brownian process noise  $\boldsymbol{\nu}_i$  of covariance  $\mathbf{R}_i$  and parameterized by a latent environmental variable  $\ell_i$  (i.e., a landmark). We assume that these measurements are acquired synchronously at a discrete sampling frequency  $1/\Delta t$  and are mutually independent.

Let  $(x(t), u(t)) \in X \times \mathcal{U}$  define a nominal (noise-free) state/control trajectory pair, that is it obeys  $\dot{x} = f(x, u)$ .

## 2.1 Optimal Estimation

When  $x$  lies on a Riemannian manifold  $X$  (not necessarily a vector space), it is convenient to consider small perturbations  $(\mathbf{x}, \mathbf{u})$  lying in the tangent space  $T_x X \times T_u \mathcal{U}$ . The small-perturbation dynamics can be approximated by linearizing  $f$  and  $h$  about  $(x, u)$ . This gives a stochastic, linear-time-varying (LTV) system

$$d\mathbf{x}(t) = \left( \mathbf{A}(x(t), u(t)) \mathbf{x}(t) + \mathbf{B}(x(t), u(t)) \mathbf{u}(t) \right) dt + \mathbf{G}(x(t), u(t)) d\mathbf{w}(t) \quad (3a)$$

$$d\mathbf{z}(t) = \mathbf{H}(x(t), \ell_i) \mathbf{x}(t) dt + d\boldsymbol{\nu}_i(t). \quad (3b)$$

A fundamental result of linear systems theory is that the covariance of the optimal unbiased estimator of the LTV system (3) is *independent* of the realization of the random processes. For a discrete-time system, the covariance evolves deterministically as given by the Extended Kalman Filter (EKF) equations

$$\mathbf{S}_k^+ = \mathbf{P}_k^{-1} + \boldsymbol{\Lambda}_k \quad (4a)$$

$$\mathbf{P}_{k+1} = \mathbf{A}_k (\mathbf{S}_{k+1}^+)^{-1} \mathbf{A}_k^T + \mathbf{G}_k \mathbf{G}_k^T \quad (4b)$$

where  $\boldsymbol{\Lambda}_k$  is the Fisher information matrix gained with respect to local state  $\mathbf{x}_k$

$$\boldsymbol{\Lambda}_k = \sum_{i=1}^N \mathbf{H}(x(t_k); \ell_i)^T \mathbf{R}_i^{-1} \mathbf{H}(x(t_k); \ell_i). \quad (5)$$

Note that (4) differs slightly from the standard EKF formulation in that the update occurs *before* the propagation step. This is due to our forthcoming definition of  $\boldsymbol{\Lambda}_k$  as describing bundled measurements over the subsequent time interval  $[t_k, t_{k+1}]$  (see Section 3). These equations implies that the covariance is a deterministic function of the system (3) and therefore of the nominal trajectory  $(x, u)$ . Moreover, if the LTV system Jacobians (3) are smooth functions of (a suitable parameterization of) the nominal trajectory,  $\mathbf{P}_k$  will be as well.

## 2.2 Trajectory Optimization

This paper focuses on a deterministic optimal control problem of the following form

$$\begin{aligned} \min_{u(\cdot)} \quad & J_c(u) + \lambda J_{\text{unc}}(u) \\ \text{subject to:} \quad & \dot{x}(t) = f(x(t), u(t)) & x(0) = x_0 \\ & u(t) \in \mathcal{U} & x(t) \in X_{\text{safe}} \end{aligned} \quad (6)$$

where we have augmented a “conventional” cost functional  $J_c$ , representing a min-energy or min-time objective, with an uncertainty penalty  $J_{\text{unc}}$ .

Note that irrespective of the choice of  $J_{\text{unc}}$ , the presence of nonlinear dynamics and/or non-convex objective function  $J_c$  are sufficient to imply that only numeric, local solutions to (6) are available in practice. Thus, choice of a non-convex  $J_{\text{unc}}$  does not make (6) fundamentally harder to solve. However, it is critical that  $J_{\text{unc}}$  be differentiable so that gradient-based methods can still be applied, and that such gradients can be efficiently computed.

### 2.3 Choices of Uncertainty Metric $J_{\text{unc}}$

A number of choices for the uncertainty term  $J_{\text{unc}}$  have been proposed, but they generally fall into three main classes. Irrespective of this choice, the goal is to produce a multi-objective optimization which smoothly trades physical trajectory cost (captured by  $J_c$ ) for estimation performance.

**Maximizing landmark visibility** A common heuristic in the case of landmark-based estimators (i.e. visual-inertial odometry) is to maximize some visibility metric [5, 12]. While this encourages onboard sensors to be pointed towards informative parts of the environment, it does not explicitly capture the observability properties of the system.

**Maximizing the Observability Gramian or Fisher-information** From a control-theoretic perspective, [8] and [14] propose maximization of metrics based on the Local Observability Gramian (LOG). The LOG is equivalent to the Fisher information (5), up to a scaling by  $R$ . Because  $\Lambda \succeq 0$  is singular for trajectories about which the system is locally unobservable, [8] and [14] propose maximization of the smallest eigenvalue  $s_1(\Lambda) \geq 0$ .

However, there are some challenges to direct maximization. Each row and column of  $\Lambda$  corresponds to a different estimated state variable, which may refer to quantities as varied as positions, velocities, and IMU biases. Maximization of individual sub-matrices (e.g., the position block) as proposed by [14] maintains consistent units of measurement, but is information-theoretically equivalent to *conditioning* on all other states (treating them all as known) and fundamentally neglects key observability properties of the system. Joint maximization, on the other hand, requires some scaling method; two different statistical approaches are presented in [13, 14]. Ultimately, direct maximization of  $\Lambda$  is a heuristic and, as pointed out by [16], can produce expensive trajectories (with respect to  $J_c$ ) that yield little improvement in estimation error.

**Minimizing posterior covariance** Following a belief-space planning formulation, we minimize the posterior estimator covariance  $P(t) \succeq 0$ . In contrast to the Fisher information (5), the posterior covariance of the EKF captures both the system dynamics and observation. Furthermore, sub-blocks of  $P(t)$  represent

the *marginal* covariances over those variables, capturing the effects of all other unknown states. Minimization over the trajectory allows the optimization to smoothly trade-off between minimizing uncertainty and conventional planning costs, even to the extent of allowing  $\Lambda$  singular at some instances. Additionally, this trade-off naturally takes into account the initial uncertainty  $P(0) = P_0$ .

In particular, if the top-left block of  $P(t)$  corresponds to the  $d \times d$  marginal covariance over position  $p$ , then choosing  $Y$  according to

$$Y = \begin{bmatrix} I_d & 0 \end{bmatrix} \implies J_{\text{unc}}(u) \triangleq \sum_{k=1}^K \text{tr}(Y P_k Y^T) = \sum_{k=1}^K \mathbb{E} \|\hat{\delta p}_k - \delta p_k\|_2^2 \quad (7)$$

that is, this choice of  $J_{\text{unc}}$  explicitly minimizes the mean-squared estimator error over position (with well-defined units of  $\text{m}^2$ ). In a sense, minimizing the posterior covariance corresponds to maximizing  $\Lambda$ , but warped and scaled *correctly* by the dynamics and prior uncertainty of the system, *without* requiring any additional tuning.

### 3 Approximating High-Rate Sensors

For high-rate sensors such as cameras, simulation of the EKF update (and subsequent gradient back-propagation) at measurement rate can be intractable for real-time planning. For this reason, we propose a computationally-efficient method to “bundle” multiple high-rate measurements into a single update. This provides a simplified proxy for the true onboard estimation scheme, facilitating efficient evaluation and optimization of trajectories.

For a given time interval  $[t_k, t_{k+1}]$  and uniform sensor rate  $1/\Delta t$ , we seek the aggregate information-to-be-gained with respect to state  $x_0 \triangleq x(0)$ . For convenience, assume that  $t_k = 0$  and the planning interval has length  $T \triangleq t_{k+1} - t_k$ . Furthermore, we focus here on the case of a single landmark, allowing us to drop the  $\ell$  argument with no loss of generality. The information-to-be-gained with respect to state  $x_0$  over the interval  $[0, T]$  can be written

$$\Lambda = \sum_{m=0}^{M-1} \Phi(t_m)^T H(x(t_m))^T R^{-1} H(x(t_m)) \Phi(t_m) \quad (8)$$

where  $M = T/\Delta t$  and  $\Phi(t)$  is the transition matrix of the local LTV system (3).

The expression (8) is equivalent to the nonlinear LOG [8, 16] and represents a “bundled” measurement as desired. However, computation requires evaluating (or approximating)  $\Phi(t)$  at  $M$  points, which is undesirable for high-rate sensors.

Instead, we leverage a Taylor-series expansion to produce a constant-time (independent of  $M$ ) approximation of (8). Let  $L_h^{(j)}$  denote the  $j^{\text{th}}$  Lie derivative of  $h$  evaluated at  $t = 0$ , and  $\nabla$  the partial derivative operator with respect to *initial* local state  $\mathbf{x}(0)$ . Then it can directly be shown that

$$H(x(t)) \Phi(t) = \frac{\partial h(x(t))}{\partial \mathbf{x}(t)} \frac{d\mathbf{x}(t)}{d\mathbf{x}(0)} = \frac{dh(x(t))}{d\mathbf{x}(0)} = \sum_{j=0}^t \frac{t^j}{j!} \nabla L_h^{(j)}. \quad (9)$$

In practice, it is sufficient to compute only the first  $r$  such terms, and substituting them into (8) yields

$$\begin{aligned}\Lambda &\approx \sum_{m=0}^{M-1} \left( \sum_{i=0}^{r-1} \frac{(t_m)^i}{i!} \nabla L_h^{(i)T} \right) \mathbf{R}^{-1} \left( \sum_{j=0}^{r-1} \frac{(t_m)^j}{j!} \nabla L_h^{(j)} \right) \\ &= \sum_{i,j=0}^{r-1} \frac{\sum_{m=0}^{M-1} (m\Delta t)^{i+j}}{i!j!} \nabla L_h^{(i)T} \mathbf{R}^{-1} \nabla L_h^{(j)} \\ &= \left[ \nabla L_h^{(0)T} \nabla L_h^{(1)T} \dots \nabla L_h^{(r-1)T} \right] (\mathbf{W} \otimes \mathbf{R}^{-1}) \left[ \nabla L_h^{(0)} \nabla L_h^{(1)} \dots \nabla L_h^{(r-1)} \right]^T\end{aligned}\quad (10)$$

where  $\otimes$  refers to the Kronecker product and the elements of the  $r \times r$  coupling matrix  $\mathbf{W}$  are

$$\mathbf{W}_{ij} \triangleq \frac{\sum_{m=0}^{M-1} (m\Delta t)^{i+j}}{i!j!} = \frac{\lambda_{i+j}}{i!j!} (\Delta t)^{i+j}. \quad (11)$$

Note that  $\lambda_s \triangleq \sum_{m=0}^{M-1} m^s$  can be pre-computed for each  $s \in \{0, 1, \dots, 2(r-1)\}$ , as  $M$  is constant in most optimization scenarios.

As desired, (10) represents a constant-time-computable approximation of (8). This summation is equivalent to *stacking* the (correlated) Lie-derivative Jacobians  $\nabla L_h^{(j)}$ , and computing the aggregate noise matrix  $\mathbf{W}$ . Crucially, the inclusion of higher-order derivatives often increases the rank of the bundled measurement, capturing the fact that states that are unobservable under a single measurement may become observable over multiple sequential sensor readings.

In contrast to the E<sup>2</sup>LOG metric presented by [14], the bundled measurement (10) explicitly approximates a *discrete*-time sensor and accounts for the measurement covariance  $\mathbf{R}$ . Furthermore, unlike [14] we do not seek to maximize this quantity directly.

For convenience in the duration of this paper,  $\mathbf{H}_k$  will denote the *whitened* bundled Jacobian over the  $k$ -th discretization interval  $[t_k, t_{k+1}]$

$$\mathbf{H}_k \triangleq (\mathbf{W} \otimes \mathbf{R}^{-1})^{\frac{1}{2}} \left[ \nabla L_h^{(0)T} \nabla L_h^{(1)T} \dots \nabla L_h^{(r-1)T} \right]^T \quad (12)$$

## 4 Differentiable Marginalization

From the previous section, we have several methods to approximate the information acquired from a particular state  $x \in X$  over the interval  $[t_i, t_{i+1}]$ . However, in the case of landmark-based sensing modalities such as visual feature tracking, the locations of the landmarks themselves are generally unknown *a priori*, and this uncertainty must be captured in the information update in order to correctly model observability. In this section, we assume that a nominal “linearization point” for each landmark  $\ell \in \mathcal{L}$  is available – this provides a well-defined local Jacobian  $\mathbf{H}(x; \ell)$ . In practice, this assumption can be met by planning against the currently-tracked set of features or by a prior distribution as described in Section 6.

Consider a suitable local parameterization  $\mathbf{l} \in \mathbb{R}^d$  of the landmark  $\ell \in \mathcal{L}$ ; then the linearized measurement residual  $\mathbf{r}$  can be written

$$\mathbf{r} = \mathbf{H}_x \mathbf{x} + \mathbf{H}_\ell \mathbf{l} + \boldsymbol{\nu}. \quad (13)$$

Of course, if the error state vector is augmented to include  $\mathbf{l}$ , then  $\mathbf{H}$  can be applied to the update in the usual way. However, this increases the error state dimension by  $d$  for each landmark, representing a quadratic growth in the system covariance matrix. This is computationally intractable when the number of landmarks is large. Some approaches, including [14, 22] simply replace  $\mathbf{H} \leftarrow \mathbf{H}_x$ , which from an information-theoretic perspective is equivalent to assuming  $\mathbf{l}$  exactly known (*conditioning*). While computationally convenient, this fails to correctly reflect the observability of the actual system and when optimized under (6) may not produce well-observable trajectories.

The information-theoretically correct approach is *marginalization*, producing an “equivalent” measurement over  $\mathbf{x}$  which captures the uncertainty over  $\mathbf{l}$ . When the distribution over  $\mathbf{l}$  is represented as a Gaussian, [11] presented a convenient solution to this approach based on the left-nullspace of  $\mathbf{H}_\ell$ . Assuming  $\mathbf{H}_\ell$  has dimension  $m \times d$  and letting  $n = m - d > 0$ , [11] showed that choosing  $m \times n$  matrix  $\mathbf{A}$  such that

$$\mathbf{A}^T \mathbf{H}_\ell = \mathbf{0}_{n \times d} \quad \text{and} \quad \mathbf{A}^T \mathbf{A} = \mathbf{I}_n \quad (14)$$

produces the linearly-transformed residual

$$\mathbf{A}^T \mathbf{r} = \mathbf{A}^T \mathbf{H}_x \mathbf{x} + \mathbf{A}^T \boldsymbol{\nu} \quad (15)$$

which is clearly independent of  $\mathbf{l}$  such that  $\mathbf{A}^T \mathbf{H}_x$  maintains maximal information over  $\mathbf{x}$ . The unitarity constraint in (14) ensures that the resulting marginalized information matrix  $\mathbf{H}_x^T \mathbf{A} \mathbf{A}^T \mathbf{H}_x$  matches the Schur complement of the full information matrix  $\mathbf{H}^T \mathbf{H}$ .

The value of this “null-space trick” [11] is that finding a satisfactory  $\mathbf{A}$  is efficiently computable via a partial SVD

$$\mathbf{H}_\ell = \mathbf{U} \begin{bmatrix} \boldsymbol{\Sigma}_1 \\ \mathbf{0}_{n \times n} \end{bmatrix} \mathbf{V}^T \implies \mathbf{A} = \mathbf{U} \begin{bmatrix} \mathbf{0}_{d \times n} \\ \mathbf{I}_n \end{bmatrix} \quad (16)$$

where  $\mathbf{U}, \mathbf{V}$  are square orthogonal matrices of dimension  $m$  and  $d$  respectively, and  $\boldsymbol{\Sigma}_1 \succ 0$  diagonal of dimension  $d$ .

In an optimization framework, we need to be able to compute gradients through this marginalization process. While the SVD is differentiable in general [17], we identify a simpler “pseudo-gradient” of  $\mathbf{A}$  such that the gradient of the resulting marginalized information matrix can be computed via the product rule

$$d(\mathbf{H}_x^T \mathbf{A} \mathbf{A}^T \mathbf{H}_x) = d\mathbf{H}_x^T \mathbf{A} \mathbf{A}^T \mathbf{H}_x + \mathbf{H}_x^T \mathbf{A} \mathbf{A}^T d\mathbf{H}_x + \mathbf{H}_x^T (\mathbf{A} d\mathbf{A}^T + d\mathbf{A} \mathbf{A}^T) \mathbf{H}_x \quad (17)$$

Such a  $d\mathbf{A}$   $m \times n$  must satisfy differentiated forms of constraints (14)

$$d\mathbf{A}^T \mathbf{H}_\ell + \mathbf{A}^T d\mathbf{H}_\ell = \mathbf{0}_{n \times d} \quad \text{and} \quad d\mathbf{A}^T \mathbf{A} + \mathbf{A}^T d\mathbf{A} = \mathbf{0}_{n \times n} \quad (18)$$



It is straightforward to verify that these conditions will be satisfied by any  $d\mathbf{A}$  such that

$$d\mathbf{A} = \mathbf{U} \begin{bmatrix} \mathbf{Z}_1 \\ \mathbf{Z}_2 \end{bmatrix} \quad (19)$$

$$\mathbf{Z}_1 = -\Sigma_1^{-1} \mathbf{V}^T d\mathbf{H}_\ell^T \mathbf{A} \quad (20)$$

$$\mathbf{Z}_2 = -\mathbf{Z}_1^T \quad (\text{skew-symmetric}) \quad (21)$$

where the inverse of diagonal  $\Sigma_1$  is trivial to compute, and  $\mathbf{Z}_2$  can conveniently be taken as  $\mathbf{0}_{n \times n}$ . In practice, this recipe is inexpensive to compute and straightforward to implement.

Note that we assume that  $\mathbf{H}_\ell$  is full rank (rank  $d$ ) in order to ensure  $\Sigma_1$  definite. The measurement bundling described in Section 3 is often sufficient to satisfy this requirement, as information from multiple observations over the interval  $[t_i, t_{i+1}]$  will render  $\mathbf{H}_\ell$  full column-rank even when the instantaneous Jacobian block is not (e.g. for vision-based sensors).

## 5 Modeling Field-of-View

Many real-world sensors, such as cameras, have limited field-of-view. Because landmarks are often distributed non-uniformly, it is important that generated trajectories point sensors towards informative regions of the environment. In the case of quadrotors with body-mounted cameras, several recent methods [5, 12] have shown that explicit optimization of a landmark visibility objective can by itself produce significant estimation improvement. In this section, we briefly describe how visibility can be represented in our posterior-covariance framework.

For a given landmark  $\ell \in \mathcal{L}$  and sensor characterized by Jacobian  $\mathbf{H}(x; \ell)$ , consider the weighting function  $\sigma$  defined as the FoV indicator  $\sigma(x, \ell) \triangleq \mathbb{1}_{\text{vis}}(x, \ell)$ . Then, for a cloud of landmarks  $\{\ell_n\}_{0 \leq n < N}$ , the information gained at state  $x$  can be computed by the sum

$$\Lambda = \sum_{i=1}^N \sigma(x, \ell^{(i)}) \mathbf{H}(x; \ell^{(i)})^T \mathbf{H}(x; \ell^{(i)}) \quad (22)$$

Of course, the indicator  $\mathbb{1}_{\text{vis}}(x, \ell)$  is discontinuous and therefore not well-suited for explicit optimization. Thus, we instead seek a *smooth*  $\sigma : X \times \mathcal{L} \mapsto [0, 1]$  which approximates  $\mathbb{1}_{\text{vis}}(x, \ell)$ .

One possible choice well-suited for a pinhole camera model is

$$\sigma(x, \ell) = \begin{cases} \frac{1}{2} (\cos a\theta + 1) & |\theta| < \theta_{\max} \\ 0 & \text{else} \end{cases} \quad (23)$$

where

$$\theta = \cos^{-1} \left( \frac{c_{\mathbf{r}}^T \hat{\mathbf{e}}}{\|c_{\mathbf{r}}\|_2} \right) \in [0, \pi] \quad (24)$$

is the angle between the optical axis  $\hat{\mathbf{e}}$  and the landmark vector  ${}^c\mathbf{r}$  in the camera frame. The scaling parameter  $a$  is chosen  $a = \pi/\theta_{\max}$ , ensuring that  $\sigma$  is continuous and differentiable. Ultimately, the best choice of  $\sigma$  will depend on the choice of sensor model and application. In the case of limited-FoV cameras [12, 22] provide some alternatives, but we found (23) sufficient for our purposes.

## 6 Handling Many Landmarks

The preceding discussion assumed a generic (albeit sufficiently differentiable) per-landmark observation function  $h(x; \ell)$ . It would then be expected that at each measurement update timestep, we must in general compute a sum (22) over all  $N$  landmarks. Similar in spirit to [22], we would like to identify a class of observation models such that we can “compress” this sum into a (near) constant-time evaluation and eliminate the complexity factor of  $N$ .

### 6.1 A Convenient Class of Measurement Models

Consider the case when there exists a parameterization of the landmark  $\mathbf{l} \in \mathbb{R}^d$  such that the observation function  $h(x; \ell)$  is *affine* in the  $\mathbf{l}$ . Then  $h$  and its Jacobian (after bundling and marginalization) can be written

$$h(x; \ell) = \mathbf{h}_0(x) + \sum_{i=1}^d l_i \mathbf{h}_i(x) \quad (25)$$

$$\mathbf{H}(x; \ell) = \mathbf{H}_0(x) + \sum_{i=1}^d l_i \mathbf{H}_i(x), \quad (26)$$

and (22) will be quadratic in the map  $\{\ell^{(n)}\}$  as

$$\begin{aligned} \Lambda(x) = & \sum_{i,j=1}^d \mathbf{H}_i(x)^T \mathbf{H}_j(x) \underbrace{\left( \sum_{n=1}^N \sigma(x, \ell^{(n)}) l_i^{(n)} l_j^{(n)} \right)}_{\triangleq a_{ij}(x)} \\ & + \sum_{i=1}^d \left( \mathbf{H}_i(x)^T \mathbf{H}_0(x) + \mathbf{H}_0(x)^T \mathbf{H}_i(x) \right) \underbrace{\left( \sum_{n=1}^N \sigma(x, \ell^{(n)}) l_i^{(n)} \right)}_{\triangleq b_i(x)} \\ & + \mathbf{H}_0(x)^T \mathbf{H}_0(x) \underbrace{\left( \sum_{n=1}^N \sigma(x, \ell^{(n)}) \right)}_{\triangleq c(x)}. \end{aligned} \quad (27)$$

From (27), it is clear the landmark dependence is confined to a  $d \times d$  matrix  $[a_{ij}(x)]$ , a length- $d$  vector  $b_i(x)$ , and a scalar  $c(x)$ , which can be thought of as feature mass coefficients. If these coefficients are computable in constant-time, so is the information  $\Lambda(x)$ . Moreover, this decomposition holds for *any* choice

of visibility function  $\sigma$ . Fortunately, there exist useful observation models for which the affine condition (25) is met. In fact, any affine function of the relative landmark position (for example in the vehicle body frame)  ${}^b\mathbf{l} = {}^w\mathbf{R}_b^T({}^w\mathbf{l} - {}^w\mathbf{p})$  has this property. While this category does *not* include perspective projection, it does include orthographic projection, which has often been used as a proxy [7]. This provides a convenient approximation for visual-SLAM systems, for which observability-based planning has already demonstrated benefit [5, 12, 21].

## 6.2 Interpretation of the Mass Coefficients

Intuitively, the mass coefficients  $(a, b, c)$  represent a *visibility-weighted* landmark distribution, with the following properties

$$[a_{ij}(x)] \succeq 0 \quad \text{and} \quad c(x) \geq 0 \quad (28)$$

It is not obvious when (or indeed if ever) these coefficients can be computed exactly in constant-time. Nonetheless, the decomposition shown in (27) lends itself to a variety of interpretations.

**An optimized implementation.** In problem instances where computing the bundled, marginalized Jacobian  $\mathbf{H}(x; \ell)$  represents non-trivial computation, (26) allows the linear components to be computed *once* at each evaluation state  $x_k$ , and iteration over  $\ell^{(i)}$  can be limited to the computation of  $(a, b, c)$ .

**Pre-computation and lookup.** When the component  $y = g(x)$  that  $\sigma$  depends on, such that  $\sigma(x, \ell) = \sigma(y, \ell)$ , lies in a low-dimensional space, this space can be discretized and corresponding values of the mass coefficients can be pre-computed. Thus computation of  $a, b, c$  can be approximated by a lookup table. In particular, [22] showed that for a particular choice of  $\sigma$  applicable to robots with a body-mounted camera, this can be achieved by discretizing solely over  $\mathbb{R}^3$ .

**A (possibly learned) prior.** In many online planning applications, landmarks are discovered and tracked in real-time as they enter the sensor’s FoV. As trajectories are often planned to the edge of (or beyond) the sensing horizon, planning strictly against the *currently*-estimated cloud may lead to myopic, undesirable behaviors such as “turning-back.” This is because the system has no mechanism to anticipate where *new* landmarks may appear. If  $a(x), b(x)$ , and  $c(x)$  are replaced by suitable *predictive* models, they may describe a convenient “prior map” allowing generalization into unknown space.

## 7 Experiments

Our approach was implemented on two example domains with limited-FoV orthographic cameras and inertial-measurement units (IMU). The first is a planar Dubin’s car, with a planar camera mounted in the forward, thrusting direction. The second is a quadrotor-based visual-inertial odometry (VIO) system in full

3D, with a forward-mounted camera. The estimation dynamics are

**Shared dynamics:**

(interpreted in  $\mathbb{R}^2$  or  $\mathbb{R}^3$ ,

respectively)

$${}^w\dot{\mathbf{p}} = {}^w\mathbf{v}$$

$${}^w\dot{\mathbf{v}} = {}^w\hat{\mathbf{a}}$$

$${}^b\dot{\boldsymbol{\omega}} = {}^b\boldsymbol{\alpha}$$

$$u \triangleq ({}^b\boldsymbol{\alpha} \ c)$$

**Dubin's car:**

$$x = ({}^w\mathbf{p} \ {}^w\mathbf{v} \ \theta \ \omega \ {}^c\mathbf{R}_b \ {}^c\mathbf{t}_b)$$

$${}^w\hat{\mathbf{a}} = c {}^w\mathbf{R}_b \mathbf{e}_1$$

$$\dot{\theta} = \omega$$

**Quadrotor:**

$$x = ({}^w\mathbf{p} \ {}^w\mathbf{v} \ {}^w\mathbf{R}_b \ \mathbf{b}_w \ \mathbf{b}_a \ {}^c\mathbf{R}_b \ {}^c\mathbf{t}_b)$$

$${}^w\dot{\mathbf{R}}_b = {}^w\mathbf{R}_b [{}^b\dot{\boldsymbol{\omega}}]_{\times}$$

$${}^b\dot{\boldsymbol{\omega}} = {}^b\boldsymbol{\omega} - \mathbf{b}_{\omega}$$

$${}^w\hat{\mathbf{a}} = {}^w\mathbf{R}_b (c\mathbf{e}_3 - \mathbf{b}_a) - g\mathbf{e}_3$$

Note that the quadrotor dynamics are IMU-driven, and depend on the unknown bias parameters ( $\mathbf{b}_w$  and  $\mathbf{b}_a \in \mathbb{R}^3$ ). Furthermore, both systems are driven by a commanded mass-normalized thrust  $c$  and angular acceleration  ${}^b\boldsymbol{\alpha}$ . The orthographic projection model given landmark  ${}^w\mathbf{l}(\ell)$  in  $\mathbb{R}^2$  or  $\mathbb{R}^3$ , respectively, is

$$h(x, \ell) = \mathbf{G}({}^c\mathbf{R}_b {}^w\mathbf{R}_b^T ({}^w\mathbf{l} - {}^w\mathbf{p}) + {}^c\mathbf{t}_b) \quad (29)$$

where  $\mathbf{G}$  is an  $1 \times 2$  or  $2 \times 3$  projection matrix  $\mathbf{G} = [\mathbf{I} \ \mathbf{0}]$  and the rigid-body transform  $({}^c\mathbf{R}_b, {}^c\mathbf{t}_b)$  describes the body-to-camera offset.

### 7.1 Validation of Measurement Bundling

To evaluate the measurement bundling described in Section 3, we can compare the approximation (10) with the explicit sum (8). For a fixed map of two landmarks in  $\mathbb{R}^2$  or  $\mathbb{R}^3$ , we consider the evolution of the stacked measurement  $z(t)$  and the aggregate information  $\Lambda$  over the interval  $[0, T]$ . The results are plotted in Fig. 1, and show that while error of course grows with time, good approximation ( $< 25\%$  error) is achieved for time horizons corresponding to the accumulation of 10 or more measurements in either case. The true value of our approximation is demonstrated in Table 1, in which computation time of the full objective are compared with and without our approximation.

### 7.2 Value of Posterior-Covariance Objective

We compared the performance of the posterior-covariance objective `post-cov` (7) to several heuristics:

- **Maximizing landmark visibility:** The method labeled `max-visibility` explicitly maximizes the *total visibility* along the trajectory, using the smooth visibility function given in (23)

$$J_{\text{unc}} \triangleq \sum_{k=1}^K \sum_{n=1}^N \sigma(x(t_k), \ell_n). \quad (30)$$

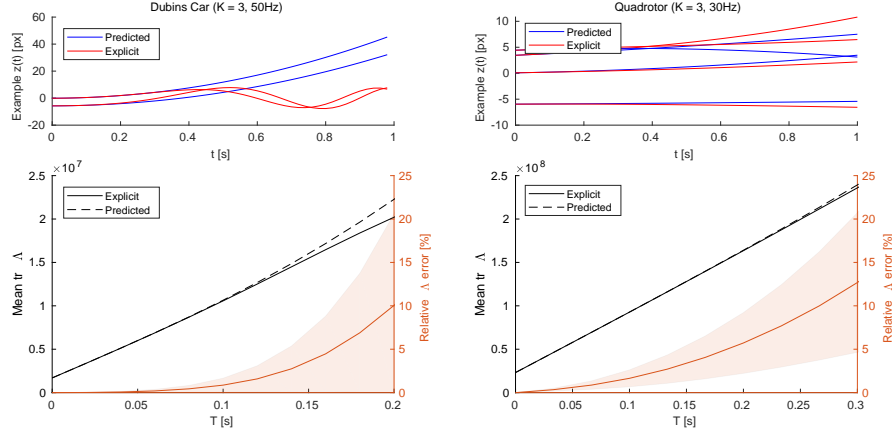


Fig. 1: Sensor approximation results for Dubin’s car [left] and quadrotor [right]. The top row shows the measurement evolution of a single random instance of a 2-landmark system. Averaged  $\Lambda$  approximation error over the interval  $[0, T]$  is plotted in the bottom row. As expected, error grows with  $T$  but remains reasonably small up to moderate time scales.

- **Max Fisher information:** Following [14], **fisher-info** maximizes the smallest eigenvalue of the cumulative Fisher information matrix (5)

$$J_{\text{unc}} \triangleq s_1 \left( \sum_{k=1}^K \Upsilon \Lambda_k \Upsilon^T \right). \quad (31)$$

Because our sensor model (29) assumes unknown landmarks, absolute position is unobservable and therefore the position sub-matrix of  $\Lambda_k$  is always zero. Therefore we chose  $\Upsilon$  to extract the velocity sub-block of  $\Lambda_k$ .

The three methods were evaluated across a batch of 50 random problem instances. In each trial, a random starting state and goal position is selected and a corresponding baseline trajectory  $(x^{(0)}(\cdot), u^{(0)}(\cdot))$  is solved for to minimize  $J_c$ . Then, this trajectory is refined under the augmented objective (6) via IPOPT [20]. As the weighting parameter  $\lambda$  is increased, the resulting trajectory  $(x^*(\cdot), u^*(\cdot))$  accepts larger increases in conventional cost  $J_c$  for more significant reductions in the uncertainty objective  $J_{\text{unc}}$ . It is worth noting that while the measurement bundling (10) and smooth FoV (23) approximations may be used during optimization, the output trajectories are evaluated using the explicit measurement rollout (8) and exact visibility indicator  $\mathbb{1}_{\text{vis}}(x, \ell)$ .

Fig. 2 shows a comparison between the **post-cov** objective and various heuristics. The choice of weighting parameter  $\lambda$  defines an effective trade-off between trajectory cost  $J_c$  increase and uncertainty reduction (measured as a relative decrease in RMSE). From these results it can be seen that the heuristic objectives do not always produce significant estimation improvement. In compar-

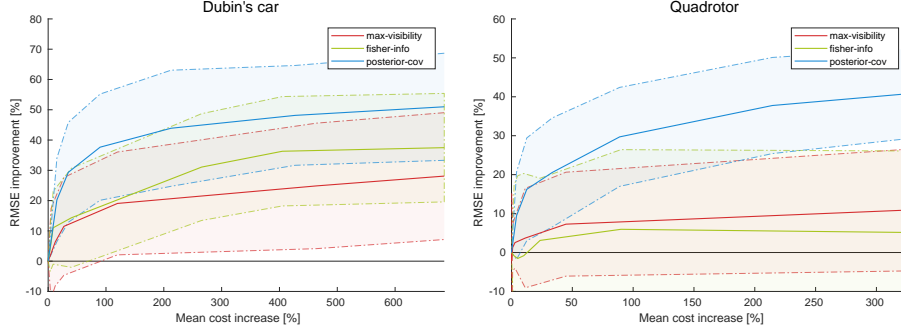


Fig. 2: Each choice of  $J_{\text{unc}}$  defines an effective trade-off curve between trajectory cost  $J_c$  and estimation improvement. We plot this curve by sweeping through the weighting parameter  $\lambda$  and aggregating results for a batch of random trials. Refinement of min-energy trajectories based on heuristic objectives (red, green) does not always yield significant estimation improvement (larger is better). In contrast, minimization of the posterior covariance directly (blue) produces better estimation improvement for the same  $J_c$  cost increase.

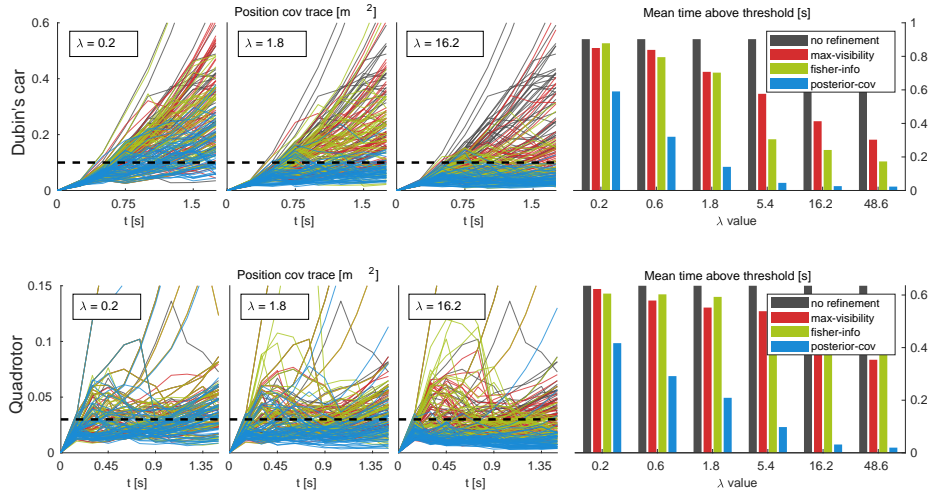


Fig. 3: Evolution of the covariance trace with varying settings of weighting parameter  $\lambda$  (normalized for similar  $J_c$  cost increase at given  $\lambda$ ). For a chosen “safety” threshold (dashed horizontal line), histograms of expected violation time are shown on the right. Without any refinement (black), uncertainty can grow without bound, but refinement under the **post-cov** objective (blue) tends to keep uncertainty bounded, even for relatively low  $\lambda$ . Heuristic (red, green) methods are less effective at ensuring safety.

Table 1: Timing results on a consumer laptop (includes gradient computation).

System	DOF	Hz	$\Delta t$	$M$	$K$	Nr. LMs	Bundling	Avg. eval
Dubin's	9	50	0.25 [s]	13	8	10	Explicit (8)	69.0 [ms]
							Taylor (10)	<b>3.9</b> [ms]
Quadrotor	21	30	0.15 [s]	5	11	50	Explicit (8)	159.4 [ms]
							Taylor (10)	<b>49.7</b> [ms]

ison, by directly optimizing the posterior-covariance, we obtain larger reductions in RMSE at moderate marginal trajectory cost.

A central goal of observability-based planning is to avoid instances where uncertainty grows to dangerous or catastrophic levels. In Fig. 3 we plot position uncertainties along a large number of simulated trajectories for the two systems. Unrefined trajectories can develop large uncertainty, often well beyond safe levels, and heuristic refinement methods do not ensure good performance in all instances (even if they do well on average). In contrast, refinement via the `post-cov` objective effectively moderates uncertainty growth across a variety of conditions, ensuring safety.

## 8 Conclusions

Our results indicate that significant estimation improvement can be achieved by explicitly considering observability during trajectory generation. While posterior-covariance minimization is not novel in itself, we address several computational challenges in the case of landmark-based estimators (i.e., visual SLAM). In doing so, we reduce algorithmic complexity from quadratic to linear in the number of landmarks and improve computation in several other ways.

In future work, we hope to produce a real-time implementation capable of online motion planning for a VIO-enabled quadrotor. Furthermore, we plan to explore learned landmark distributions in the context of the quadratic decomposition (27) – that is, learning the mass coefficients  $a, b, c$  directly. This would make computation of  $\Lambda$  truly constant-time and enable *anticipation* of new landmarks based on a learned prior.

## 9 Acknowledgment

This work was supported by the Education Office at the Charles Stark Draper Laboratory and by ARL DCIST under Cooperative Agreement Number W911NF-17-2-0181.

## References

1. Arneberg, J., Tal, E., Karaman, S.: Guidance laws for partially-observable interception based on linear covariance analysis. In: Proc. IEEE Conf. Int. Rob. Sys. (IROS), pp. 4185–4191. IEEE (2018)

2. Bry, A., Roy, N.: Rapidly-exploring random belief trees for motion planning under uncertainty. In: Proc. IEEE Conf. Robot. Autom. (ICRA), pp. 723–730. IEEE (2011)
3. Conticelli, F., Bicchi, A., Balestrino, A.: Observability and nonlinear observers for mobile robot localization. IFAC Proceedings Volumes **33**(27), 663–668 (2000)
4. Elisha, Y.B., Indelman, V.: Active online visual-inertial navigation and sensor calibration via belief space planning and factor graph based incremental smoothing. In: Proc. IEEE Conf. Int. Rob. Sys. (IROS), pp. 2616–2622. IEEE (2017)
5. Falanga, D., Foehn, P., Lu, P., Scaramuzza, D.: PAMPC: Perception-aware MPC for quadrotors. In: Proc. IEEE Conf. Int. Rob. Sys. (IROS), pp. 1–8. IEEE (2018)
6. Indelman, V., Carlone, L., Dellaert, F.: Planning in the continuous domain: A generalized belief space approach for autonomous navigation in unknown environments. Int. J. of Robotics Research **34**(7), 849–882 (2015)
7. Kanade, T., Morris, D.D.: Factorization methods for structure from motion. Philosophical Transactions of the Royal Society of London **356**(1740), 1153–1173 (1998)
8. Krener, A.J., Ide, K.: Measures of unobservability. In: Conf. on Dec. and Control (CDC), pp. 6401–6406. IEEE (2009)
9. Mariottini, G.L., Morbidi, F., Prattichizzo, D., Vander Valk, N., Michael, N., Pappas, G., Daniilidis, K.: Vision-based localization for leader–follower formation control. IEEE Transactions on Robotics **25**(6), 1431–1438 (2009)
10. Mellinger, D., Kumar, V.: Min-snap trajectory generation and control for quadrotors. In: Proc. IEEE Conf. Robot. Autom. (ICRA), pp. 2520–2525. IEEE (2011)
11. Mourikis, A.I., Roumeliotis, S.I.: A multi-state constraint kalman filter for vision-aided inertial navigation. In: Proc. IEEE Conf. Robot. Autom. (ICRA), pp. 3565–3572. IEEE (2007)
12. Murali, V., Spasojevic, I., Guerra, W., Karaman, S.: Perception-aware trajectory generation for aggressive quadrotor flight using differential flatness. In: American Control Conference (ACC) (2019)
13. Nobre, F., Heckman, C.: Learning to calibrate: Reinforcement learning for guided calibration of visualinertial rigs. Int. J. of Robotics Research (2019)
14. Preiss, J.A., Hausman, K., Sukhatme, G.S., Weiss, S.: Simultaneous self-calibration and navigation using trajectory optimization. Int. J. of Robotics Research (2018)
15. Prentice, S., Roy, N.: The belief roadmap: Efficient planning in belief space by factoring the covariance. Int. J. of Robotics Research **28**(11-12), 1448–1465 (2009)
16. Raffeisakhaei, M., Chakravorty, S., Kumar, P.: The use of the observability gramian for partially observed path planning problems. pp. 1523–1528. IEEE (2017)
17. Townsend, J.: Differentiating the singular value decomposition. <https://j-towns.github.io/papers/svd-derivative.pdf> (2016). Accessed: 2019-05-14
18. Van Den Berg, J., Abbeel, P., Goldberg, K.: LQG-MP: Optimized path planning for robots with motion uncertainty and imperfect state information. Int. J. of Robotics Research **30**(7), 895–913 (2011)
19. Van Den Berg, J., Patil, S., Alterovitz, R.: Motion planning under uncertainty using iterative local optimization in belief space. Int. J. of Robotics Research **31**(11), 1263–1278 (2012)
20. Wächter, A., Biegler, L.T.: On the implementation of an interior-point filter line-search algorithm for large-scale nonlinear programming. Mathematical programming **106**(1), 25–57 (2006)
21. Zhang, Z., Scaramuzza, D.: Perception-aware receding horizon navigation for MAVs. In: Proc. IEEE Conf. Robot. Autom. (ICRA), pp. 2534–2541. IEEE (2018)
22. Zhang, Z., Scaramuzza, D.: Beyond point clouds: Fisher information field for active visual localization. In: Proc. IEEE Conf. Robot. Autom. (ICRA). IEEE (2019)